

Article

Continuous Measurements of Temporal and Vertical Variations in Atmospheric CO₂ and Its δ¹³C in and above a Subtropical Plantation

Changhua Chen ¹, Xuefa Wen ^{1,2,3} , Jingyuan Wang ^{1,*} and Qingjun Guo ^{1,2}

¹ Key Laboratory of Ecosystem Network Observation and Modelling, Center for Environmental Remediation, Institute of Geographic Sciences and Natural Resources Research, Chinese Academy of Sciences, Beijing 100101, China; chench.14b@igsnr.ac.cn (C.C.); wenxf@igsnr.ac.cn (X.W.); guoqj@igsnr.ac.cn (Q.G.)

² College of Resources and Environment, University of Chinese Academy of Sciences, Beijing 100190, China

³ Yanshan Earth Critical Zone and Surface Fluxes Research Station, University of Chinese Academy of Sciences, Beijing 101408, China

* Correspondence: wangjy@igsnr.ac.cn; Tel.: +86-136-9367-1280

Abstract: Atmospheric CO₂ dynamics in forest ecosystems are dependent on interactions between photosynthesis, respiration, and turbulent mixing processes; however, the carbon isotopic composition of atmospheric CO₂ (δ¹³C) is not well established due to limited measurement reports. In this study, a seven-inlet profile system with a Picarro analyzer was developed to conduct continuous in situ measurements of CO₂ and its δ¹³C in and above a subtropical plantation from 2015 to 2017. Results showed that ecosystem CO₂ concentration was the lowest in the afternoon and reached its peak at dawn, which mirrored variations in its δ¹³C in and above the canopy. Inverse seasonal variations were apparent between CO₂ and its δ¹³C in and above the canopy, and δ¹³C was positive during the peak growing season and negative at other times. Diel and seasonal variations in ecosystem CO₂ and its δ¹³C were mainly affected by the vapor pressure deficit, followed by photosynthetic active radiation, temperature, and the enhanced vegetation index in and above the canopy; however, environmental and physiological factors had reverse or no effects near the forest floor. Nocturnal gradients of vertical variations in atmospheric CO₂ and its δ¹³C were greater than diurnal variations due to weak turbulent mixing under more stable atmospheric conditions overnight. These results implicate that photosynthesis and respiration dominated CO₂ dynamics above the canopy, while CO₂ recycling by photosynthesis and turbulent mixing changed CO₂ dynamics in the canopy.

Keywords: stable carbon isotope; CO₂; climate–vegetation feedbacks; atmospheric stability; photosynthesis; respiration; forest carbon sink



Citation: Chen, C.; Wen, X.; Wang, J.; Guo, Q. Continuous Measurements of Temporal and Vertical Variations in Atmospheric CO₂ and Its δ¹³C in and above a Subtropical Plantation. *Forests* **2021**, *12*, 584. <https://doi.org/10.3390/f12050584>

Academic Editors: Jordi Voltas, Juan Pedro Ferrio and Tatiana A. Shestakova

Received: 3 April 2021

Accepted: 5 May 2021

Published: 7 May 2021

Publisher's Note: MDPI stays neutral with regard to jurisdictional claims in published maps and institutional affiliations.



Copyright: © 2021 by the authors. Licensee MDPI, Basel, Switzerland. This article is an open access article distributed under the terms and conditions of the Creative Commons Attribution (CC BY) license (<https://creativecommons.org/licenses/by/4.0/>).

1. Introduction

Forest ecosystems fix approximately one-third of the current anthropogenic CO₂ emissions from the atmosphere [1,2]; hence, an accurate assessment of forest carbon sink is important to better understand the global carbon budget [3,4]. The stable carbon isotope composition of ecosystem CO₂ (δ¹³C) is a powerful tool for tracing carbon cycling and its exchange with the atmosphere [5]. CO₂ dynamics in forest ecosystems are the results of canopy photosynthesis, respiration of different components (leaf, stem, root, and soil microbes), and turbulent mixing processes [6,7]; however, patterns of δ¹³C are not well established due to limited measurements, particularly during the day [8]. Higher CO₂ concentration is always associated with more negative δ¹³C of forest air [8,9]. Isotope ratio infrared spectroscopy (IRIS) technology has been used to continuously observe ecosystem CO₂ and its δ¹³C [8–11], providing insight into the underlying mechanisms of δ¹³C dynamics in forest ecosystems [12,13].

Biogenic CO₂ has a significant imprint on diurnal variations in ecosystem δ¹³C [14]. Mass discrimination or isotope effects, which will cause changes in isotope abundance,

result in isotopic fractionation during chemical, physical and biological processes [15]. Figure 1 shows that photosynthetic discrimination ($^{13}\Delta$) against heavier ^{13}C leads to isotopic enrichment of forest canopy $^{13}\text{CO}_2$ during the daytime [16,17]. Conversely, post-photosynthetic fractionation during plant respiration [14,18], metabolic fractionation from soil microbial respiration [19,20], and diffusion fractionation of soil efflux [21,22] cause isotopic depletion of the ecosystem CO_2 . The refixation of respired CO_2 affects the $\delta^{13}\text{C}$ of source CO_2 during canopy photosynthesis [6]. Furthermore, the troposphere exchanges $^{12}\text{CO}_2$ and $^{13}\text{CO}_2$ with ecosystem air by turbulent mixing [23], which varies the relative contributions of ecosystem photosynthesis and component respiration during the daytime; limited mixing among these component respiration creates vertical stratification of ecosystem CO_2 and its $\delta^{13}\text{C}$ under stable nighttime conditions [24]. However, forest CO_2 dynamics in a hilly ecosystem are generally influenced by complex terrain [25]; local flows and weather conditions will also influence on the short-term variations in $\delta^{13}\text{C}$ of forest CO_2 .

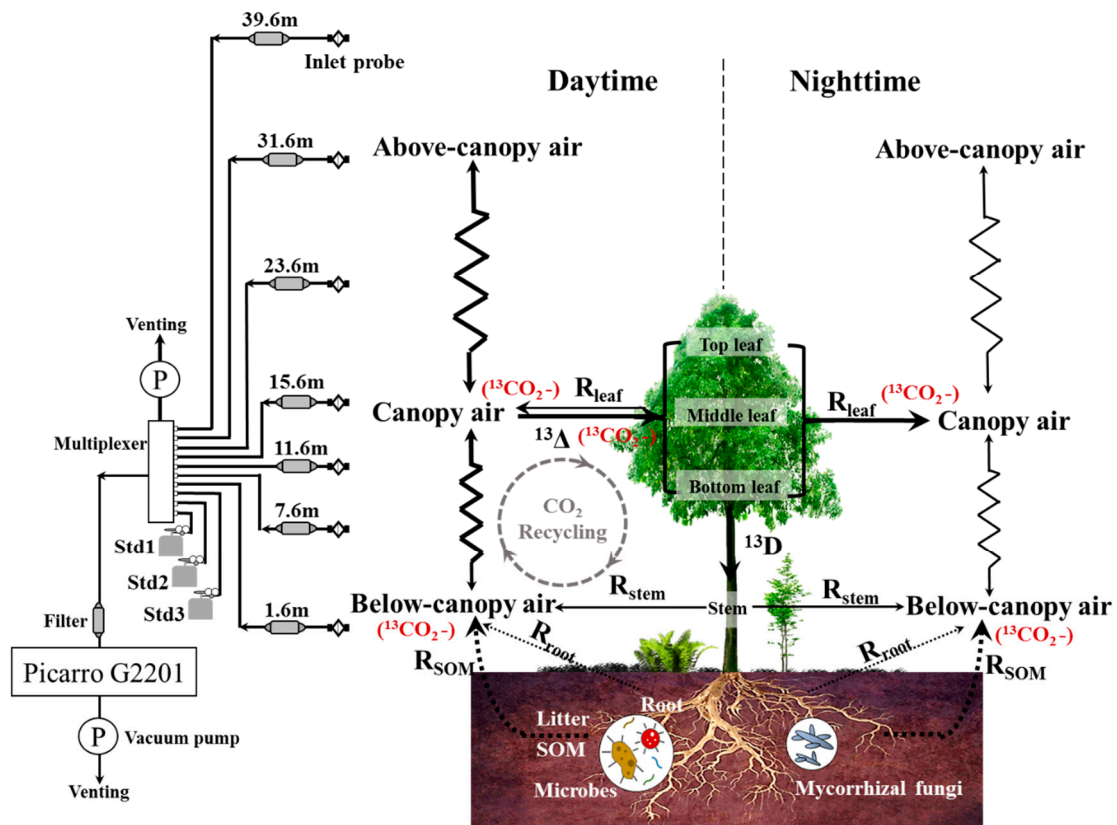


Figure 1. The processes contributing to forest CO_2 and its stable carbon isotope ($\delta^{13}\text{C}$), and the multi-inlet profile system used to sample CO_2 and its $\delta^{13}\text{C}$ in and above the canopy. $^{13}\Delta$ represents photosynthetic carbon isotope discrimination, R represents the respiration of different components, and ^{13}D represents the carbon isotopic disequilibrium between ecosystem photosynthesis and respiration. SOM represents soil organic matter. The gray dashed lines represent the recycling of respired ecosystem CO_2 by photosynthesis, black broken lines represent turbulent mixing, and black dotted lines represent the CO_2 diffusion of soil respiration ignoring chemoautotrophic and anaplerotic fixation. Std1, Std2, and Std3 represent three standard gases of the profile system. Picarro G2201 represents the Picarro G2201-i CO_2 $\delta^{13}\text{C}$ analyzer (Picarro Inc., Sunnyvale, CA, USA).

The response of forest ecosystem CO_2 and its $\delta^{13}\text{C}$ to environmental stress and physiological activity may differ below and within the canopy. Ecosystem photosynthesis, respiration, and turbulent mixing are all associated with variations in canopy structure, temperature, moisture conditions, etc. [26,27]. There are empirical relationships between climate variation and the ecosystem response, which are negatively correlated with soil

moisture (SWC) and precipitation, and positively correlated with vapor pressure deficit (VPD), air temperature (T_a), and photosynthetic active radiation (PAR). $^{13}\Delta$ increases with reductions in water content in boreal forest mosses [28], and there is a time lag between carbon isotopic composition of ecosystem respiration (δ_R) and VPD [29–32]. However, the relative contributions of ecosystem photosynthesis and respiration and their isotopic signatures vary with phenological activity and environmental disturbance [25,26]; they respond differently to precipitation [33,34] and drought [35,36], suggesting that there may be fundamental differences in the environmental factors and physiological activity at the canopy spatial scale. Some studies reported that $\delta^{13}\text{C}$ values of forest respiration were significantly correlated with VPD within the canopy [30–32,37], and soil moisture near the forest floor [25].

Subtropical forest ecosystems in the East Asian monsoon region have a high CO_2 uptake, similar to that of North American and European temperate forests [38]. We developed a multi-inlet $^{12}\text{CO}_2$ and $^{13}\text{CO}_2$ profile system combined with a Picarro analyzer to conduct in situ measurements of atmospheric CO_2 and its $\delta^{13}\text{C}$ in and above the canopy in a subtropical plantation from 2015 to 2017. This study aims to (1) examine the temporal (diel and seasonal) and vertical variations of atmospheric CO_2 and its $\delta^{13}\text{C}$ in and above the forest ecosystem, and (2) elucidate the effects of environmental and physiological factors and atmospheric conditions on temporal and vertical variations.

2. Materials and Methods

2.1. Site Description

Field measurements were conducted at the ChinaFLUX Qianyanzhou site ($26^\circ 44' 52''$ N, $115^\circ 03' 47''$ E, elevation 102 m) in Southeastern China. This hilly region is strongly influenced by the subtropical East Asian monsoon climate. The subtropical plantation was planted around 1985 and is dominated by *Pinus massoniana* Lamb., *Pinus elliottii* Englem., and *Cunninghamia lanceolata* Hook., with a canopy height of approximately 16–18 m. The dominant shrubs are *Loropetalum chinense* Oliv. and *Adinandra mellettii* Hook. et Am., with canopy heights below 5 m. The herbaceous layer includes *Dicranopteris dichotoma* (Thunb.) Bernh., *Dryopteris peninsulae* Kitag., and *Woodwardia japonica* (L. f.) Sm., with heights below 1 m. The litter layer is present year-round, and has a thickness of approximately 5 cm. The soil type is mainly acid red soil, and the bulk density of the surface soil (0–40 cm) is 1.57 g cm^{-3} . CO_2 emissions from soil inorganic carbon were not considered.

2.2. Profile System In Situ Measurements

The mixing ratios of $^{12}\text{CO}_2$ and $^{13}\text{CO}_2$ were measured using a multi-inlet profile system from 14 January 2015 (Figure 1). The multi-inlet profile system was comprised of a Picarro G2201-i CO_2 $\delta^{13}\text{C}$ analyzer (Picarro Inc., Sunnyvale, CA, USA) using wavelength-scanned cavity ring-down spectroscopy, seven air sampling inlets, and three standard gases (Std1, Std2, and Std3). The distribution of sampling inlets at 1.6, 7.6, 11.6, 15.6, 23.6, 31.6, and 39.6 m formed a vertical atmospheric profile below, within, and above the canopy.

In a sampling sequence, the three standard gases were each scanned for five minutes; then, the seven ambient air inlets were selected in turn for three minutes each and scanned 14 times. The standard gases and sampling air were pumped continuously at a flow rate of 0.03 L min^{-1} into the analyzer and signals were recorded at 0.3 Hz with standard temperature and pressure. Allan variance analysis showed that the G2201-i analyzer had the best precision for CO_2 (0.01 ppm) and $\delta^{13}\text{C}$ (0.01‰) at 7600 s [35]. Some data during the summer of 2017 were missing due to extreme thunderstorm events. A more detailed instrument configuration can be found in the literature [11].

2.3. Calibration of Forest CO_2 and Its $\delta^{13}\text{C}$

A three-point linear calibration scheme was applied to correct the measured ecosystem atmosphere $^{12}\text{CO}_2$ and $^{13}\text{CO}_2$ and standard gases from 2015 to 2017 [11]. The corrected

atmospheric $^{12}\text{CO}_2$ and $^{13}\text{CO}_2$ were then used to calculate atmospheric CO_2 and its $\delta^{13}\text{C}$ as follows:

$$\text{CO}_2 = \frac{^{12}\text{CO}_2 + ^{13}\text{CO}_2}{1 - f} \quad (1)$$

and

$$\delta^{13}\text{C} = \frac{^{13}\text{CO}_2}{^{12}\text{CO}_2} \times 1000 \quad (2)$$

where CO_2 is the total mixing ratio ($\mu\text{mol mol}^{-1}$), f is the fraction of all CO_2 isotopomers (0.00474), $\delta^{13}\text{C}$ represents the delta notation of isotopic mixing ratios (‰), and R_{VPDB} is the standard molar ratio of 0.0111797.

The differences (mean \pm SD) between the calibrated and true values of Std1, Std2, and Std3 ranged from -1.63 ± 0.13 to $3.09 \pm 0.28 \mu\text{mol mol}^{-1}$ for CO_2 and from -0.027 ± 0.075 to $0.017 \pm 0.048\text{‰}$ for $\delta^{13}\text{C}$ (Table 1). The strong performance of the multi-inlet CO_2 and its $\delta^{13}\text{C}$ profile sampling system ensured the long-term stability and accuracy of observations.

Table 1. Validation data for the multi-inlet CO_2 and its $\delta^{13}\text{C}$ vertical profile sampling system.

Year	CO_2 ($\mu\text{mol mol}^{-1}$)			$\delta^{13}\text{C}$ (‰)		
	Std1	Std2	Std3	Std1	Std2	Std3
2015	-1.59 ± 0.17	3.00 ± 0.34	1.42 ± 0.14	0.006 ± 0.049	-0.009 ± 0.077	0.004 ± 0.030
2016	-1.63 ± 0.13	3.09 ± 0.28	-1.46 ± 0.11	0.017 ± 0.048	-0.027 ± 0.075	0.011 ± 0.030
2017	-1.62 ± 0.13	3.06 ± 0.28	1.45 ± 0.10	0.011 ± 0.051	-0.017 ± 0.079	0.009 ± 0.032

2.4. Meteorological Measurements and Atmospheric Conditions

Meteorological measurements were completed with an eddy covariance (EC) flux system which was mounted on a tower at 39.6 m. The EC system was comprised of an open-path $\text{CO}_2/\text{H}_2\text{O}$ analyzer (Model Li-7500, Licor Inc., Lincoln, NE, USA) and a 3D sonic anemometer (Model CSAT3, Campbell Scientific Inc., Logan, UT, USA). Meteorological measurements from 2015 to 2017 provided the photosynthetic active radiation (PAR), air temperature (T_a), humidity (RH), wind velocity (WS) and direction, precipitation, soil temperature (T_s), and soil moisture (SWC). Meteorological data were averaged at half hourly intervals. More detailed data processing and quality control are provided in [39].

We used two estimates to describe atmospheric stability: the friction wind velocity (u^*) and scaled Obukhov length atmospheric stability (ξ , $= (z - d)/L$). The u^* was calculated at a height of 39.6 m using mean horizontal and vertical wind speeds. ξ was determined using the displacement height (d), and the Obukov length (L) was calculated.

2.5. Vegetation and Aridity Indexes and Statistical Analyses

The enhanced vegetation index (EVI) is considered to be a physiological factor of forest carbon flux that is more responsive to leaf area and canopy biophysical characteristics [40]. We obtained 16-EVI data at a spatial resolution of 250 m from the MOD13Q1 and MYD13Q1 product subsets [41], merged the two subsets by time, and then linearly interpolated the data to obtain daily values from 2015 to 2017.

Budyko's aridity index (AI) was expressed as the ratio of monthly precipitation and potential evapotranspiration, where $\text{AI} < 1$ indicates periods of drought stress [42], and potential evapotranspiration is calculated in the same way as in [43].

Correlations were calculated using the Pearson method to analyze the relationships between environmental and physiological factors and atmospheric CO_2 and its $\delta^{13}\text{C}$ in and above the forest ecosystem. Statistical significance was fixed to p -value < 0.001 .

3. Results

3.1. Environmental and Biological Factors

Figure 2 shows seasonal variations of AI, and environmental (PAR, Ta, Ts, VPD, and SWC) and biological factors (EVI) between 2015 and 2017. Averaged across all three years, the AI from July to October was less than 1 under the influence of the subtropical anticyclone, indicating seasonal drought stress during this period (Figure 2a). Environmental factors and vegetation physiological activity varied with season (Figure 2b–f). The three-year averages of PAR, Ta, Ts, VPD, SWC, and EVI were $18.49 \pm 12.35 \text{ mol m}^{-2} \text{ d}^{-1}$, $18.54 \pm 8.06 \text{ }^\circ\text{C}$, $18.20 \pm 6.46 \text{ }^\circ\text{C}$, $0.41 \pm 0.38 \text{ KPa}$, $0.24 \pm 0.06 \text{ m}^3 \text{ m}^{-3}$, and $0.36 \pm 0.09 \text{ m}^2 \text{ m}^{-2}$, respectively. Annual precipitation was highest in 2015 (1755.8 mm), but its annual SWC was lowest due to intense evaporation.

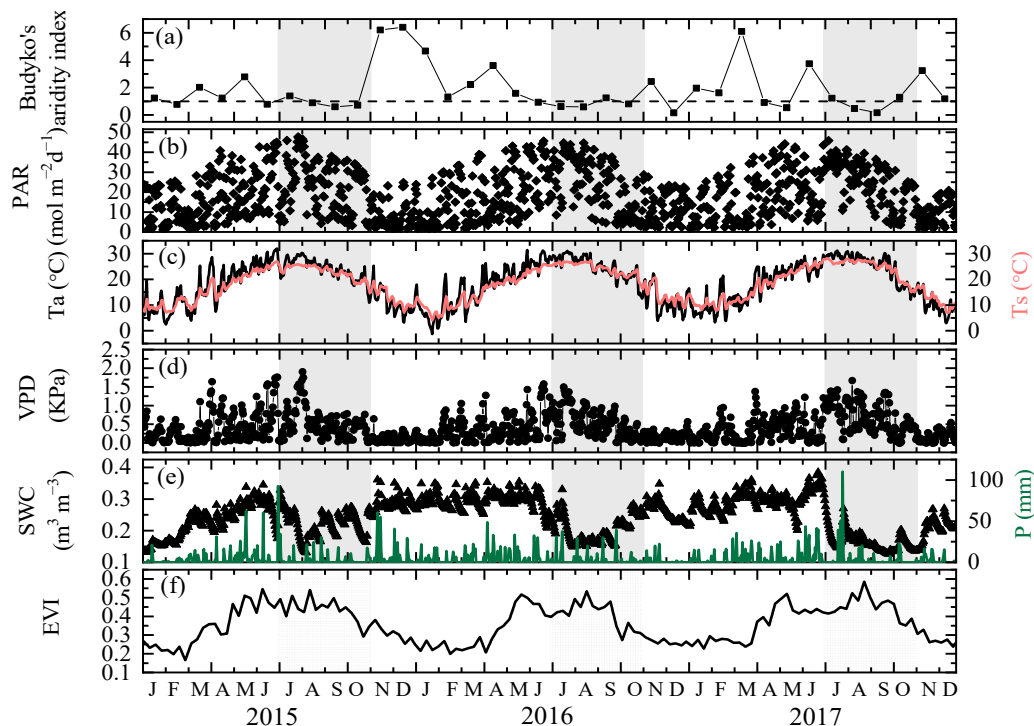


Figure 2. Seasonal variations in monthly (a) Budyko's aridity index (AI), daily (b) photosynthetically active radiation at a height of 39.6 m (PAR), (c) canopy air temperature at height of 11.6 m (Ta) and soil temperature at a depth of 5 cm (Ts), (d) atmospheric vapor pressure deficit (VPD) at height of 11.6 m, (e) soil moisture at a depth of 5cm (SWC) and precipitation, and (f) the enhanced vegetation index (EVI) between 2015 and 2017. Gray areas represent seasonal drought periods (July–October) based on the AI values.

3.2. Temporal and Vertical Variations of Ecosystem CO₂ and Its $\delta^{13}\text{C}$

Figure 3 shows the monthly mean diel variation of half hourly ecosystem CO₂ and its $\delta^{13}\text{C}$ below (1.6 and 7.6 m), within (11.6 and 15.6 m) and above (23.6, 31.6, and 39.6 m) the canopy (2015–2017); the original time series of atmospheric CO₂ and its $\delta^{13}\text{C}$ at each individual height are shown in Figures S1 and S2, respectively. Atmospheric CO₂ decreases and its $\delta^{13}\text{C}$ becomes more positive with canopy height; diel CO₂ mirrors variations in its $\delta^{13}\text{C}$ at different canopy heights (Figure 3). The diel pattern of CO₂ is lowest in the afternoon (14:00–15:00) and peaks at dawn (5:00–6:00). Conversely, peak $\delta^{13}\text{C}$ occurred in the afternoon, and was the lowest in the early morning.

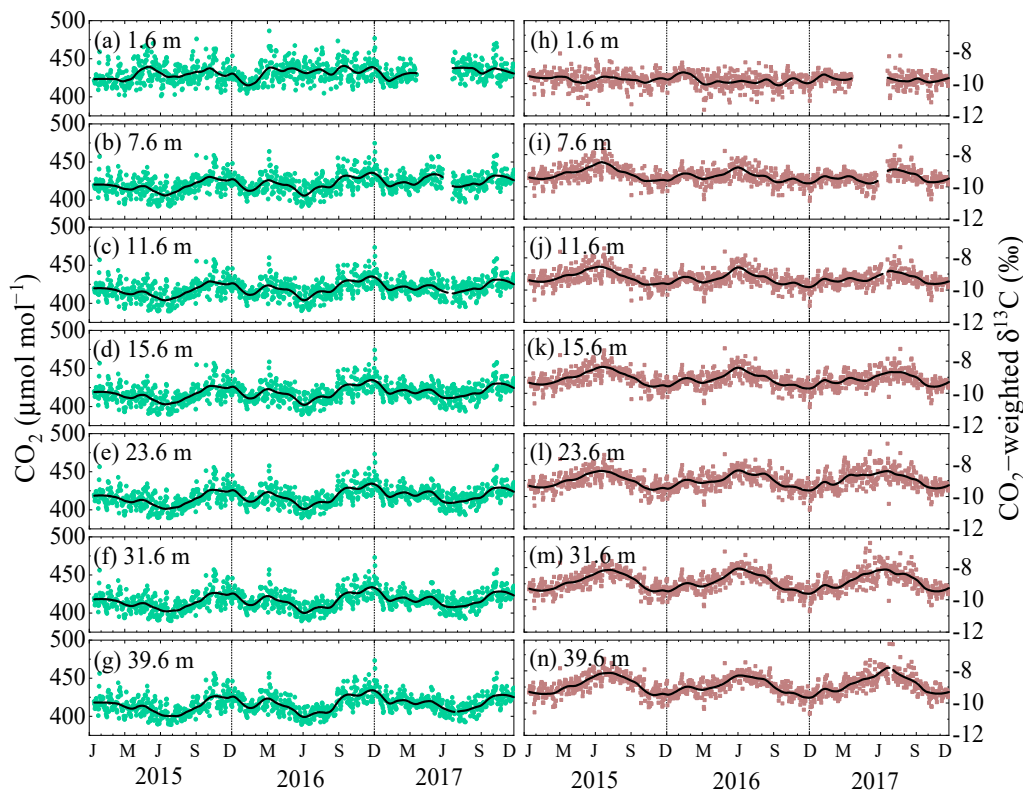


Figure 4. Seasonal variations in daily ecosystem CO_2 (a–g) and its weighted $\delta^{13}\text{C}$ (h–n) below (1.6 and 7.6 m), within (11.6 and 15.6 m) and above (23.6, 31.6, and 39.6 m) the canopy (2015–2017). The black curves represent locally weighted smoothing lines.

3.3. Effects of Atmospheric Conditions on Variations in Ecosystem CO_2 and Its $\delta^{13}\text{C}$

We selected a rainy (DOY137–140 in 2015) and drought (DOY215–218 in 2015) period as typical study periods to analyze the impact of different atmospheric conditions during the daytime and overnight. Black areas in Figure 5 show the occurrence of stable conditions ($u^* < 0.4 \text{ m s}^{-1}$, $\xi > 0.1$) during the daytime (10:00–16:00) and night (22:00–4:00) for both the rainy and drought periods. Due to weak turbulence in the nocturnal flow, the stable atmospheric conditions overnight lasted longer than during the day for both the rainy and drought periods. However, nocturnal atmospheric conditions were more stable during the rainy period, which might be related to the local circulations in hilly terrain during the drought period.

Figure 6 shows vertical variations in atmospheric CO_2 , its $\delta^{13}\text{C}$, and wind speed (WS) for each day during the rainy and drought periods. Nocturnal gradients of vertical variations in forest ecosystem CO_2 and its $\delta^{13}\text{C}$ were greater than diurnal variations, and daytime ecosystem CO_2 throughout the canopy was similar to that of CO_2 in the well-mixed atmosphere above the canopy. Vertical variations in ecosystem CO_2 and its $\delta^{13}\text{C}$ during the rainy period were more significant than those in the drought period both during the day and overnight. Moreover, forest ecosystem CO_2 increased and its $\delta^{13}\text{C}$ became more negative as the WS decreased below the canopy because high CO_2 from soil autotrophic and heterotrophic respiration was diffused and concentrated near the forest floor.

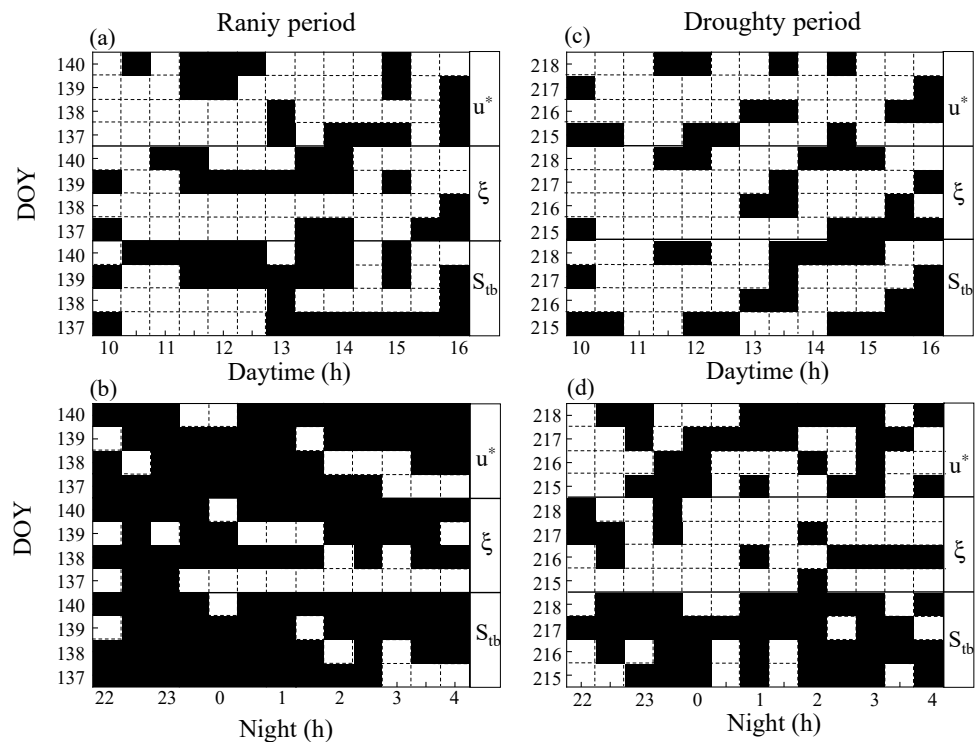


Figure 5. Binary matrix of half hourly friction velocity (u^*), atmospheric stability (ξ), and atmospheric conditions (S_{tb}) as determined by the two stability indicators during the daytime (10:00–16:00) and overnight (22:00–4:00) for the typical rainy and droughty periods. Black areas show time periods under stable conditions ($u^* < 0.4 \text{ m s}^{-1}$, $\xi > 0.1$). (a,b) are results during daytime and overnight for the rainy period, (c,d) are results during daytime and overnight for the droughty period.

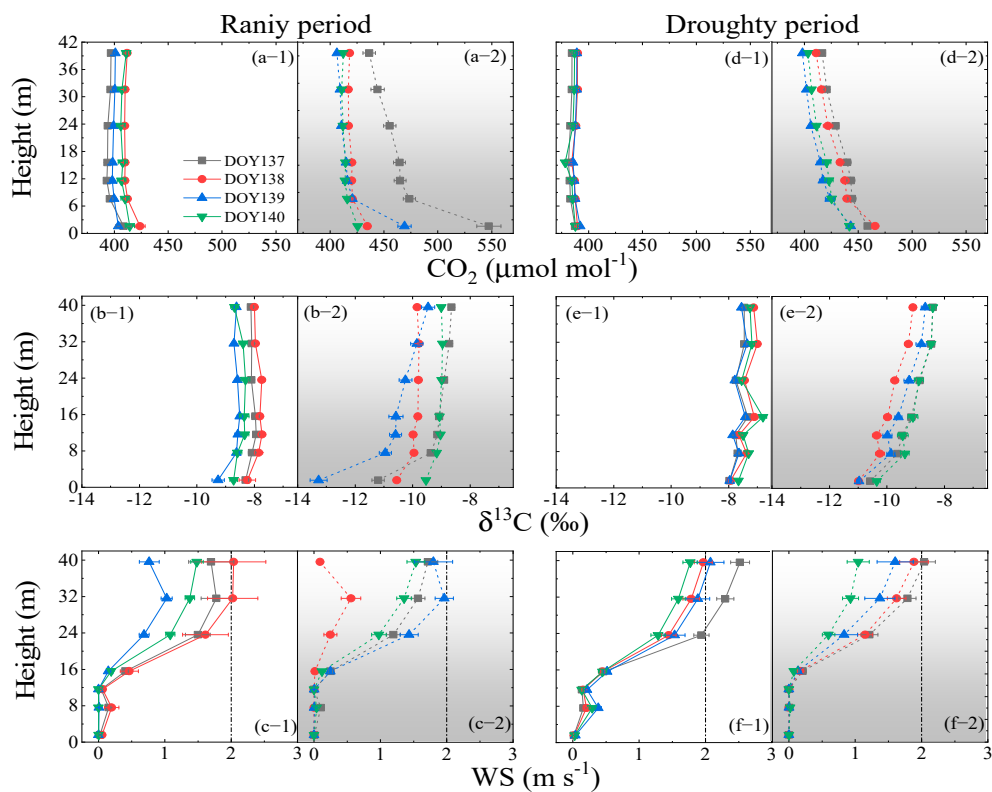


Figure 6. Daily mean vertical variations of ecosystem CO_2 (a,d), its $\delta^{13}\text{C}$ (b,e) and wind speed (WS) (c,f) for each day during the typical rainy (DOY 137–140) and droughty (DOY 215–218) periods. White and grey areas represent the diurnal (10:00–16:00) and nocturnal (22:00–4:00) results, respectively.

3.4. Effects of Environmental and Biological Factors on Variations in Ecosystem CO₂ and Its δ¹³C

Figure 7 shows the Pearson correlations of atmospheric CO₂ and its δ¹³C with environmental (PAR, Ta, Ts, VPD, RH, and SWC) and biological factors (EVI) at diel (Figure 7a,b) and seasonal (Figure 7c,d) time scales (2015–2017). Atmospheric CO₂ within and above the canopy was significantly negatively correlated with photosynthetically active radiation (PAR), temperature (Ta and Ts), and EVI ($p < 0.001$) at the diel and seasonal scales, and was positively correlated with moisture conditions (VPD, SWC, and RH). Accordingly, the δ¹³C of atmospheric CO₂ had a significant inverse correlation with these factors. The effects of environmental and biological factors on atmospheric CO₂ and its δ¹³C varied with canopy height. At diel scales, PAR, VPD, and RH had more obvious effects on canopy (15.6 m) CO₂ and its δ¹³C compared to other layers; correlations of other factors at the seasonal scale became stronger with canopy height.

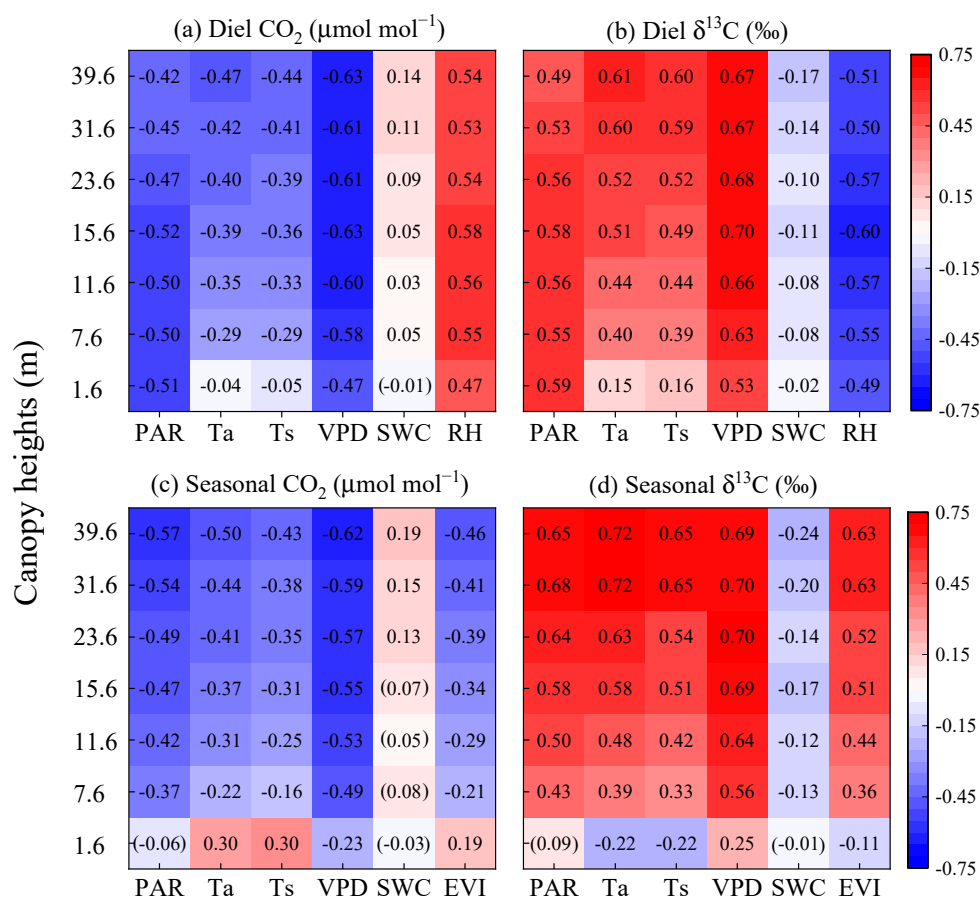


Figure 7. Correlation matrix of daily CO₂ and its δ¹³C at different canopy layers with half hourly (a,b) and daily (c,d) environmental and biological factors between 2015 and 2017. Pearson correlation coefficients in brackets are not significant ($p > 0.001$).

There were reverse effects of temperature (Ta and Ts) and EVI on CO₂ and its δ¹³C near the forest floor (1.6 m), and correlations of PAR and SWC at this layer were low or insignificant (Figure 7). This indicates that the response of forest ecosystem CO₂ and its δ¹³C to environmental stress and physiological activity varies at canopy spatial scales. The overall effects of environmental and biological factors were VPD > RH > PAR > Ta > Ts > SWC for CO₂ and its δ¹³C at the diel scale, and VPD > PAR > Ta > EVI > Ts > SWC for CO₂ and VPD > Ta > PAR > Ts > EVI > SWC for δ¹³C at the seasonal scale.

4. Discussion

4.1. Diel Variations and Effects of $\delta^{13}\text{C}$ of Ecosystem CO_2

The diel cycle of ecosystem atmospheric CO_2 and its $\delta^{13}\text{C}$ essentially reflect short-term variations in ecosystem photosynthesis, respiration, and their related carbon isotopic fractionation and environmental factors. Observed patterns in $\delta^{13}\text{C}$ of ecosystem CO_2 showed distinct diurnal variations in and above a subalpine forest [8]; values of $\delta^{13}\text{C}$ reached its maximum in the afternoon and minimum in the morning with values ranging from -11.01 to -7.94‰ near the floor of the deciduous forest [10]. Diurnal variations in photosynthetic discrimination ($^{13}\Delta$) in C_3 plants generally range from 10 to 35‰ [9,44,45], and high $^{13}\Delta$ values have been measured or modeled at dawn and dusk [44,46]. Ecosystem exchange studies have often assumed that there was no short-term variation in the carbon isotope of ecosystem respiration (δ_{R}) between day and night; hence, the intercept of the nightly Keeling plot [47] or the slope of the nightly Miller-Tans plot [48] reflected the daily δ_{R} values. However, considering changes in the substrate of autotrophic respiration at the diel scale and the relative contribution of components to ecosystem respiration, some studies have found that there was a more positive trend in the evening and a gradual decrease overnight [30,49], a general pattern trending to negative [50] or positive [51], or no short-term variation in δ_{R} [52]. Short-term and diurnal variations ranged from 3 to 10‰ in forest ecosystem respiration [14,53].

There were deviations in the phases of the diel cycle between ecosystem CO_2 and its $\delta^{13}\text{C}$ because of the carbon isotopic disequilibrium ($^{13}\text{D} = \delta_{\text{A}} - \delta_{\text{R}}$) between ecosystem photosynthesis (δ_{A}) and δ_{R} . The ^{13}D value determined the weights of ecosystem CO_2 resulting from isotopic enrichment by $^{13}\Delta$, and isotopic depletion by post-photosynthetic fractionation in plants and metabolic fractionation from soil microbes. Observational and modeling studies have frequently produced estimates of $^{13}\text{D} > 0$ at the ecosystem scale [44,45,54], suggesting that isotopic depletion during ecosystem respiration was stronger than the enrichment by $^{13}\Delta$. Thus, ecosystem $\delta^{13}\text{C}$ trending to positive would peak earlier than CO_2 in the afternoon. Conversely, the maximum diel variation in ecosystem CO_2 occurred at dawn (Figure 3), and the minimum of $\delta^{13}\text{C}$ occurred earlier than the CO_2 peaks because the $^{13}\Delta$ values were high in the initial stages of photosynthesis. In summary, the peak and trough of ecosystem $\delta^{13}\text{C}$, in theory, occurred earlier than that of CO_2 in the diel cycle.

4.2. Seasonal Variations and Effects of $\delta^{13}\text{C}$ of Ecosystem CO_2

Seasonal variations in ecosystem atmospheric CO_2 and its $\delta^{13}\text{C}$ generally reflected seasonal fluctuations of background CO_2 , ecosystem photosynthesis, and respiration. Since the Industrial Revolution, fossil fuel burning and land use changes have decreased $\delta^{13}\text{C}$ values in the troposphere CO_2 , and the increase in $^{13}\Delta$ slows down this declining trend [55,56]. The background values of $\delta^{13}\text{C}$ of ecosystem CO_2 at two typical atmospheric stations in China (Waliguan and Shangdianzi) were more positive in summer than in spring [57]. Meanwhile, there were seasonal variations in ecosystem photosynthesis and respiration. The $^{13}\Delta$ values were obtained by gas exchange measurements and Farquhar's model [16]. Wingate et al. [9] reported that broad seasonal changes in $^{13}\Delta$ were reflected in the carbon isotopic composition of the stem, soil, and ecosystem in a maritime pine stand (*Pinus pinaster* Ait.); however, they became decoupled from soil respiration during rainy periods. Similar to seasonal variations in background CO_2 [31,58], the seasonal variations in $\delta^{13}\text{C}$ of forest ecosystem CO_2 were more than 7‰ [30,59].

Forest understory provided important contributions to ecosystem respiration [13]; CO_2 recycling from the soil and understory changed atmospheric CO_2 and its $\delta^{13}\text{C}$ in the canopy. The mechanisms of seasonal $^{13}\Delta$ are still unclear due to a lack of field observations; however, Choi et al. [60] reported that $^{13}\Delta$ was increased by irrigation due to increased stomatal and/or mesophyll conductance in a loblolly pine stand (*Pinus taeda* L.), Wingate et al. [9] showed that rain events caused $^{13}\Delta$ to increase above 20‰ in a maritime pine stand (*Pinus pinaster* Ait.), and another study further indicated that precipitation controlled the latitude distribution of $^{13}\Delta$ across the world [61]. In this study, seasonal variations in

ecosystem atmospheric CO₂ and its δ¹³C were affected by VPD, PAR, Ta, and EVI, and there were reverse effects for Ta and EVI near the forest floor (Figure 7). Schaeffer et al. [25] also found stronger correlations between δ_R within the canopy and VPD, and δ_R near the ground and SWC in a subalpine coniferous forest. The effects of SWC on ecosystem CO₂ and its δ¹³C were not significant in this study, as forest ecosystems may use the VPD to regulate the effects of moisture conditions on vegetation photosynthesis, or the groundwater buffering of plant uptake [43] to mitigate drought stress.

4.3. Vertical Variations and Effects of δ¹³C of Ecosystem CO₂

Vertical variations in ecosystem CO₂ and its δ¹³C formed the “canopy effect” [24], in which ecosystem CO₂ increases, while its δ¹³C is progressively isotopically depleted towards the forest floor [8,29]. Heterogeneity was apparent in the distribution of ecosystem components and the allocation of resources and environmental factors at the canopy spatial scale [62,63]. Reasons for the vertical profile of δ¹³C of ecosystem CO₂ are as follows: (1) turbulent mixing between canopy CO₂ and isotopically enriched CO₂ from the troposphere; (2) PAR becomes progressively weaker near the floor, causing an increase in the CO₂ concentration ratio in the intercellular space to canopy air (C_i/C_a); thus, ¹³Δ values are increased [17,64] and δ_A is depleted; and (3) the isotopic dilution effect of CO₂ below the canopy due to soil respiration.

Atmospheric conditions impacted turbulent mixing between the isotopically enriched background CO₂ and depleted biogenic CO₂. The forest atmosphere under stable nighttime conditions was stratified with poor mixing within and below the canopy, forming a distinct profile structure of forest ecosystem CO₂ and its δ¹³C (Figure 6). The atmospheric boundary layer brought high momentum down to the canopy top under unstable conditions, which impacted the vertical profiles of turbulence moments and integral length scales within and above the canopy [65]. In this study, the subtropical high controlled the drought period; consequently, more sunny days and drainage flow with the development of temperature inversions influenced the transport of CO₂ in complex terrain [25]. Furthermore, forest CO₂ dynamics are dependent on interactions between photosynthesis, respiration, and turbulent mixing processes (Figure 1). It is likely that photosynthesis and respiration dominated CO₂ dynamics above the canopy, while CO₂ recycling by photosynthesis and turbulent mixing changed CO₂ dynamics in the canopy. Further investigations are needed to quantify the effects of photosynthesis, respiration, and turbulent mixing processes to the forest CO₂ dynamics.

5. Conclusions

In this study, we developed a multi-inlet profile system with a Picarro analyzer to continuously measure CO₂ and its δ¹³C below, within, and above the canopy in a subtropical plantation from 2015 to 2017. Diel and seasonal patterns of ecosystem CO₂ mirrored variations in δ¹³C at seven different canopy heights. Temporal variations in ecosystem CO₂ and its δ¹³C were affected by VPD > PAR > T > EVI; however, environmental and physiological factors displayed reverse or no effects near the forest floor. Nocturnal gradients of vertical variations in ecosystem CO₂ and its δ¹³C were greater than diurnal variations due to weak turbulent mixing under stable conditions, and vertical gradients during the rainy period were more significant compared to those during the drought period, possibly due to drainage flow during the drought period.

Supplementary Materials: The following are available online at <https://www.mdpi.com/article/10.3390/f12050584/s1>, Figure S1: The original time series of ecosystem CO₂ at seven heights in and above a subtropical plantation between 2015 and 2017, Figure S2: The original time series of δ¹³C of ecosystem CO₂ at seven heights in and above a subtropical plantation between 2015 and 2017.

Author Contributions: C.C. and X.W. contributed to fieldwork; C.C. analyzed all data and prepared the manuscript. C.C., X.W., J.W., and Q.G. reviewed manuscript. All authors have read and agreed to the published version of the manuscript.

Funding: This research was funded by National Natural Science Foundation of China (31901133, 41830860, and 42077302) and China Postdoctoral Science Foundation (2019M660779).

Data Availability Statement: The datasets generated and/or analyzed during the current study are available from the corresponding author on reasonable request.

Conflicts of Interest: The authors declare no conflict of interest.

References

- Grassi, G.; House, J.; Dentener, F.; Federici, S.; den Elzen, M.; Penman, J. The key role of forests in meeting climate targets requires science for credible mitigation. *Nat. Clim. Chang.* **2017**, *7*, 220–226. [[CrossRef](#)]
- Pan, Y.D.; Birdsey, R.A.; Fang, J.; Houghton, R.; Kauppi, P.E.; Kurz, W.A.; Phillips, O.L.; Shvidenko, A.; Lewis, S.L.; Canadell, J.G.; et al. A Large and Persistent Carbon Sink in the World's Forests. *Science* **2011**, *333*, 988–993. [[CrossRef](#)]
- Le Quere, C.; Peters, G.P.; Andres, R.J.; Andrew, R.M.; Boden, T.A.; Ciais, P.; Friedlingstein, P.; Houghton, R.A.; Marland, G.; Moriarty, R.; et al. Global carbon budget 2013. *Earth Syst. Sci. Data* **2014**, *6*, 235–263. [[CrossRef](#)]
- Walden, L.L.; Fontaine, J.B.; Ruthrof, K.X.; Matusick, G.; Harper, R.J.; Hardy, G.E.S.J. Carbon consequences of drought differ in forests that resprout. *Glob. Chang. Biol.* **2019**, *25*, 1653–1664. [[CrossRef](#)]
- Flanagan, L.B.; Ehleringer, A.R. Ecosystem-atmosphere CO₂ exchange: Interpreting signals of change using stable isotope ratios. *Trends Ecol. Evol.* **1998**, *13*, 10–14. [[CrossRef](#)]
- Sternberg, L.D.L.O. A Model to Estimate Carbon Dioxide Recycling in Forests Using ¹³C/¹²C Ratios and Concentrations of Ambient Carbon-Dioxide. *Agric. For. Meteorol.* **1989**, *48*, 163–173. [[CrossRef](#)]
- Lloyd, J.; Kruijt, B.; Hollinger, D.Y.; Grace, J.; Francey, R.J.; Wong, S.C.; Kelliher, F.M.; Miranda, A.C.; Farquhar, G.D.; Gash, J.H.C.; et al. Vegetation effects on the isotopic composition of atmospheric CO₂ at local and regional scales: Theoretical aspects and a comparison between rain forest in amazonia and a boreal forest in Siberia. *Aust. J. Plant Physiol.* **1996**, *23*, 371–399. [[CrossRef](#)]
- Bowling, D.R.; Burns, S.P.; Conway, T.J.; Monson, R.K.; White, J.W.C. Extensive observations of CO₂ carbon isotope content in and above a high-elevation subalpine forest. *Global Biogeochem. Cycles* **2005**, *19*. [[CrossRef](#)]
- Santos, E.; Wagner-Riddle, C.; Lee, X.; Warland, J.; Brown, S.; Staebler, R.; Bartlett, P.; Kim, K. Use of the isotope flux ratio approach to investigate the C¹⁸O¹⁶O and ¹³CO₂ exchange near the floor of a temperate deciduous forest. *Biogeosciences* **2012**, *9*, 2385–2399. [[CrossRef](#)]
- Wingate, L.; Ogee, J.; Burrell, R.; Bosc, A.; Devaux, M.; Grace, J.; Loustau, D.; Gessler, A. Photosynthetic carbon isotope discrimination and its relationship to the carbon isotope signals of stem, soil and ecosystem respiration. *New Phytol.* **2010**, *188*, 576–589. [[CrossRef](#)]
- Chen, C.; Pang, J.; Wei, J.; Wen, X.; Sun, X. Inter-comparison of three models for δ¹³C of respiration with four regression approaches. *Agric. For. Meteorol.* **2017**, *247*, 229–239. [[CrossRef](#)]
- Braendholt, A.; Ibrom, A.; Steenberg Larsen, K.; Pilegaard, K. Partitioning of ecosystem respiration in a beech forest. *Agric. For. Meteorol.* **2018**, *252*, 88–98. [[CrossRef](#)]
- Paul-Limoges, E.; Wolf, S.; Eugster, W.; Hortnagl, L.; Buchmann, N. Below-canopy contributions to ecosystem CO₂ fluxes in a temperate mixed forest in Switzerland. *Agric. For. Meteorol.* **2017**, *247*, 582–596. [[CrossRef](#)]
- Brüggemann, N.; Gessler, A.; Kayler, Z.; Keel, S.G.; Badeck, F.; Barthel, M.; Boeckx, P.; Buchmann, N.; Brugnoli, E.; Esperschütz, J.; et al. Carbon allocation and carbon isotope fluxes in the plant-soil-atmosphere continuum: A review. *Biogeosciences* **2011**, *8*, 3457–3489. [[CrossRef](#)]
- Meier-Augenstein, W. Isotope Effects, Mass Discrimination and Isotopic Fractionation. In *Stable Isotope Forensics*; John Wiley & Sons: Hoboken, NJ, USA, 2010; pp. 10–15.
- Badeck, F.W.; Tcherkez, G.; Nogues, S.; Piel, C.; Ghashghaie, J. Post-photo synthetic fractionation of stable carbon isotopes between plant organs—A widespread phenomenon. *Rapid Commun. Mass Spectrom.* **2005**, *19*, 1381–1391. [[CrossRef](#)]
- Farquhar, G.D.; O'Leary, M.H.; Berry, J.A. On the Relationship Between Carbon Isotope Discrimination and the Inter-cellular Carbon Dioxide Concentration in Leaves. *Aust. J. Plant Physiol.* **1982**, *9*, 121. [[CrossRef](#)]
- Von Caemmerer, S.; Millgate, A.; Farquhar, G.D.; Furbank, R.T. Reduction of ribulose-1,5-bisphosphate carboxylase/oxygenase by antisense RNA in the C₄ plant *Flaveria bidentis* leads to reduced assimilation rates and increased carbon isotope discrimination. *Plant Physiol.* **1997**, *113*, 469–477. [[CrossRef](#)]
- Werner, C.; Gessler, A. Diel variations in the carbon isotope composition of respired CO₂ and associated carbon sources: A review of dynamics and mechanisms. *Biogeosciences* **2011**, *8*, 2437–2459. [[CrossRef](#)]
- Apostel, C.; Herschbach, J.; Bore, E.K.; Spielvogel, S.; Kuzyakov, Y.; Dippold, M.A. Food for microorganisms: Position-specific ¹³C labeling and ¹³C-PLFA analysis reveals preferences for sorbed or necromass C. *Geoderma* **2018**, *312*, 86–94. [[CrossRef](#)]
- Moyes, A.B.; Gaines, S.J.; Siegwolf, R.T.W.; Bowling, D.R. Diffusive fractionation complicates isotopic partitioning of autotrophic and heterotrophic sources of soil respiration. *Plant Cell Environ.* **2010**, *33*, 1804–1819. [[CrossRef](#)]
- Van Asperen, H.; Warneke, T.; Sabbatini, S.; Hopker, M.; Nicolini, G.; Chiti, T.; Papale, D.; Böhm, M.; Notholt, J. Diel variation in isotopic composition of soil respiratory CO₂ fluxes: The role of non-steady state conditions. *Agric. For. Meteorol.* **2017**, *234*, 95–105. [[CrossRef](#)]

23. Zappa, C.J.; McGillis, W.R.; Raymond, P.A.; Edson, J.B.; Hints, E.J.; Zemmelen, H.J.; Dacey, J.W.H.; Ho, D.T. Environmental turbulent mixing controls on air-water gas exchange in marine and aquatic systems. *Geophys. Res. Lett.* **2007**, *34*. [[CrossRef](#)]
24. Martinelli, L.A.; Almeida, S.; Brown, I.F.; Moreira, M.Z.; Victoria, R.L.; Sternberg, L.S.L.; Ferreira, C.A.C.; Thomas, W.W. Stable carbon isotope ratio of tree leaves, boles and fine litter in a tropical forest in Rondonia, Brazil. *Oecologia* **1998**, *114*, 170–179. [[CrossRef](#)]
25. Schaeffer, S.M.; Anderson, D.E.; Burns, S.P.; Monson, R.K.; Sun, J.; Bowling, D.R. Canopy structure and atmospheric flows in relation to the $\delta^{13}\text{C}$ of respired CO_2 in a subalpine coniferous forest. *Agric. For. Meteorol.* **2008**, *148*, 592–605. [[CrossRef](#)]
26. Migliavacca, M.; Reichstein, M.; Richardson, A.D.; Mahecha, M.D.; Cremonese, E.; Delpierre, N.; Galvagno, M.; Law, B.E.; Wohlfahrt, G.; Black, T.A.; et al. Influence of physiological phenology on the seasonal pattern of ecosystem respiration in deciduous forests. *Glob. Chang. Biol.* **2015**, *21*, 363–376. [[CrossRef](#)] [[PubMed](#)]
27. Buchmann, N.; Kao, W.Y.; Ehleringer, J.R. Carbon dioxide concentrations within forest canopies—Variation with time, stand structure, and vegetation type. *Glob. Chang. Biol.* **1996**, *2*, 421–432. [[CrossRef](#)]
28. Williams, T.G.; Flanagan, L.B. Effect of changes in water content on photosynthesis, transpiration and discrimination against ^{13}C and $\text{C}^{18}\text{O}^{16}\text{O}$ in *Pleurozium* and *Sphagnum*. *Oecologia* **1996**, *108*, 38–46. [[CrossRef](#)] [[PubMed](#)]
29. Riveros-Iregui, D.A.; Hu, J.; Burns, S.P.; Bowling, D.R.; Monson, R.K. An interannual assessment of the relationship between the stable carbon isotopic composition of ecosystem respiration and climate in a high-elevation subalpine forest. *J. Geophys. Res. Biogeosci.* **2011**, *116*. [[CrossRef](#)]
30. Werner, C.; Unger, S.; Pereira, J.S.; Maia, R.; David, T.S.; Kurz-Besson, K.; David, J.S.; Maguas, C. Importance of short-term dynamics in carbon isotope ratios of ecosystem respiration ($\delta^{13}\text{C}$) in a Mediterranean oak woodland and linkage to environmental factors. *New Phytol.* **2006**, *172*, 330–346. [[CrossRef](#)]
31. Shim, J.H.; Powers, H.H.; Pereira, J.S.; Maia, R.; David, T.S.; Kurz-Besson, C.; David, J.S.; Maguas, C. The role of interannual, seasonal, and synoptic climate on the carbon isotope ratio of ecosystem respiration at a semiarid woodland. *Glob. Chang. Biol.* **2011**, *17*, 2584–2600. [[CrossRef](#)]
32. Ekblad, A.; Bostrom, B.; Holm, A.; Comstedt, D. Forest soil respiration rate and $\delta^{13}\text{C}$ is regulated by recent above ground weather conditions. *Oecologia* **2005**, *143*, 136–142. [[CrossRef](#)]
33. Chen, J.; Luo, Y.Q.; Xia, J.; Shi, Z.; Jiang, L.; Niu, S.; Zhou, X.; Cao, J. Differential responses of ecosystem respiration components to experimental warming in a meadow grassland on the Tibetan Plateau. *Agric. For. Meteorol.* **2016**, *220*, 21–29. [[CrossRef](#)]
34. Dorrepaal, E.; Toet, S.; van Logtestijn, R.S.P.; Swart, E.; van de Weg, M.J.; Callaghan, T.V.; Aerts, T. Carbon respiration from subsurface peat accelerated by climate warming in the subarctic. *Nature* **2009**, *460*, 616–619. [[CrossRef](#)]
35. Miao, G.F.; Noormets, A.; Domec, J.-C.; Fuentes, M.; Trettin, C.C.; Sun, G.; McNulty, S.G.; King, J.S. Hydrology and microtopography control carbon dynamics in wetlands: Implications in partitioning ecosystem respiration in a coastal plain forested wetland. *Agric. Forest Meteorol.* **2017**, *247*, 343–355. [[CrossRef](#)]
36. Doughty, C.E.; Metcalfe, D.B.; Girardin, C.A.J.; Farfan Amezcua, F.; Galiano Carbera, D.; Huaraca Huasco, W.; Silva-Espejo, J.E.; Araujo-Murakami, A.; da Costa, M.C.; Rocha, W.; et al. Drought impact on forest carbon dynamics and fluxes in Amazonia. *Nature* **2015**, *519*, 78–82. [[CrossRef](#)] [[PubMed](#)]
37. Pang, J.P.; Wen, X.F.; Sun, X.; Huang, K. Intercomparison of two cavity ring-down spectroscopy analyzers for atmospheric $^{13}\text{CO}_2/^{12}\text{CO}_2$ measurement. *Atmos. Meas. Tech.* **2016**, *9*, 3879–3891. [[CrossRef](#)]
38. Yu, G.R.; Chen, Z.; Peng, C.; Ciais, P.; Wang, Q.; Li, X.; Zhu, X. High carbon dioxide uptake by subtropical forest ecosystems in the East Asian monsoon region. *Proc. Natl. Acad. Sci. USA* **2014**, *111*, 4910–4915. [[CrossRef](#)]
39. Wen, X.F.; Wang, H.M.; Wang, J.-L.; Yu, G.-R.; Sun, X.-M. Ecosystem carbon exchanges of a subtropical evergreen coniferous plantation subjected to seasonal drought, 2003–2007. *Biogeosciences* **2010**, *7*, 357–369. [[CrossRef](#)]
40. Huete, A.; Didan, K.; Miura, T.; Rodriguez, E.P.; Gao, X.; Ferreira, L.G. Overview of the radiometric and biophysical performance of the MODIS vegetation indices. *Remote Sens. Environ.* **2002**, *83*, 195–213. [[CrossRef](#)]
41. The Oak Ridge National Laboratory Distributed Active Archive Center (ORNL DAAC). MODIS and VIIRS Land Products Global Subsetting and Visualization Tool. 2018. Available online: https://daac.ornl.gov/cgi-bin/dsviewer.pl?ds_id=1379 (accessed on 13 November 2020).
42. Budyko, M.I. *Climate and Life*; Academic Press: New York, NY, USA, 1974.
43. Yang, B.; Wen, X.; Sun, X. Seasonal variations in depth of water uptake for a subtropical coniferous plantation subjected to drought in an East Asian monsoon region. *Agric. For. Meteorol.* **2015**, *201*, 218–228. [[CrossRef](#)]
44. Chen, C.; Wei, J.; Wen, X.; Sun, X.; Guo, Q. Photosynthetic Carbon Isotope Discrimination and Effects on Daytime NEE Partitioning in a Subtropical Mixed Conifer Plantation. *Agric. For. Meteorol.* **2019**, *272*, 143–155. [[CrossRef](#)]
45. Zobitz, J.M.; Burns, S.P.; Reichstein, M.; Bowling, D.R. Partitioning net ecosystem carbon exchange and the carbon isotopic disequilibrium in a subalpine forest. *Glob. Chang. Biol.* **2008**, *14*, 1785–1800. [[CrossRef](#)]
46. Wingate, L.; Seibt, U.; Moncrieff, J.B.; Jarvis, P.G.; Lloyd, J. Variations in ^{13}C discrimination during CO_2 exchange by *Picea sitchensis* branches in the field. *Plant Cell Environ.* **2007**, *30*, 600–616. [[CrossRef](#)]
47. Keeling, C.D. The Concentration and Isotopic Abundances of Atmospheric Carbon Dioxide in Rural Areas. *Geochim. Cosmochim. Acta* **1958**, *13*, 322–334. [[CrossRef](#)]
48. Miller, J.B.; Tans, P.P.; White, J.W.C.; Conway, T.J.; Vaughn, B.W. The atmospheric signal of terrestrial carbon isotopic discrimination and its implication for partitioning carbon fluxes. *Tellus B Chem. Phys. Meteorol.* **2003**, *55*, 197–206. [[CrossRef](#)]

49. Bowling, D.R.; Sargent, S.D.; Tanner, B.D.; Ehleringer, J.R. Tunable diode laser absorption spectroscopy for stable isotope studies of ecosystem-atmosphere CO₂ exchange. *Agric. For. Meteorol.* **2003**, *118*, 1–19. [[CrossRef](#)]
50. Zhang, J.; Griffis, T.J.; Baker, J.M. Using continuous stable isotope measurements to partition net ecosystem CO₂ exchange. *Plant Cell Environ.* **2006**, *29*, 483–496. [[CrossRef](#)] [[PubMed](#)]
51. Unger, S.; Maguas, C.; Pereira, J.S.; Aires, L.M.; David, T.S.; Werner, C. Disentangling drought-induced variation in ecosystem and soil respiration using stable carbon isotopes. *Oecologia* **2010**, *163*, 1043–1057. [[CrossRef](#)] [[PubMed](#)]
52. Kodama, N.; Barnard, R.L.; Salmon, Y.; Weston, C.; Ferrio, J.P.; Holst, J.; Werner, R.A.; Saurer, M.; Rennenberg, H.; Buchmann, N.; et al. Temporal dynamics of the carbon isotope composition in a *Pinus sylvestris* stand: From newly assimilated organic carbon to respired carbon dioxide. *Oecologia* **2008**, *156*, 737–750. [[CrossRef](#)]
53. Sun, W.; Resco, V.; Williams, D.G. Environmental and physiological controls on the carbon isotope composition of CO₂ respired by leaves and roots of a C₃ woody legume (*Prosopis velutina*) and a C₄ perennial grass (*Sporobolus wrightii*). *Plant Cell Environ.* **2012**, *35*, 567–577. [[CrossRef](#)]
54. Bowling, D.R.; Ballantyne, A.P.; Miller, J.B.; Burns, S.P.; Conway, T.J.; Menzer, O.; Stephens, O.O.; Vaughn, B.H. Ecological processes dominate the ¹³C land disequilibrium in a Rocky Mountain subalpine forest. *Glob. Biogeochem. Cycles* **2014**, *28*. [[CrossRef](#)]
55. Graven, H.; Keeling, R.F.; Rogelj, J. Changes to Carbon Isotopes in Atmospheric CO₂ Over the Industrial Era and into the Future. *Glob. Biogeochem. Cycles* **2020**, *34*. [[CrossRef](#)] [[PubMed](#)]
56. Graven, H.; Allison, C.E.; Etheridge, D.M.; Hammer, S.; Keeling, R.F.; Levin, I.; Meijer, H.A.J.; Rubino, M.; Tans, P.P.; Trudinger, C.M.; et al. Compiled records of carbon isotopes in atmospheric CO₂ for historical simulations in CMIP6. *Geosci. Model Dev.* **2017**, *10*, 4405–4417. [[CrossRef](#)]
57. Liu, L.; Zhou, L.; Vaughn, B.; Miller, J.B.; Brand, W.A.; Rothe, M.; Xia, L. Background variations of atmospheric CO₂ and carbon-stable isotopes at Waliguan and Shangdianzi stations in China. *J. Geophys. Res. Atmos.* **2014**, *119*, 5602–5612. [[CrossRef](#)]
58. Scartazza, A.; Mata, C.; Matteucci, G.; Yakir, D.; Moscatello, S.; Brugnoli, E. Comparisons of δ¹³C of photosynthetic products and ecosystem respiratory CO₂ and their responses to seasonal climate variability. *Oecologia* **2004**, *140*, 340–351. [[CrossRef](#)] [[PubMed](#)]
59. McDowell, N.G.; Bowling, D.R.; Schauer, A.; Irvine, J.; Bond, B.J.; Law, B.E.; Ehleringer, J.R. Associations between carbon isotope ratios of ecosystem respiration, water availability and canopy conductance. *Glob. Chang. Biol.* **2004**, *10*, 1767–1784. [[CrossRef](#)]
60. Choi, W.J.; Chang, S.X.; Allen, H.L.; Kelting, D.L.; Ro, H.-M. Irrigation and fertilization effects on foliar and soil carbon and nitrogen isotope ratios in a loblolly pine stand. *For. Ecol. Manag.* **2005**, *213*, 90–101. [[CrossRef](#)]
61. Basu, S.; Ghosh, S.; Sanyal, P. Spatial heterogeneity in the relationship between precipitation and carbon isotopic discrimination in C₃ plants: Inferences from a global compilation. *Glob. Planet. Chang.* **2019**, *176*, 123–131. [[CrossRef](#)]
62. Ghashghaie, J.; Badeck, F.W. Opposite carbon isotope discrimination during dark respiration in leaves versus roots—A review. *New Phytol.* **2014**, *201*, 751–769. [[CrossRef](#)]
63. Wegener, F.; Beyschlag, W.; Werner, C. Dynamic carbon allocation into source and sink tissues determine within-plant differences in carbon isotope ratios. *Funct. Plant Biol.* **2015**, *42*, 620–629. [[CrossRef](#)]
64. Brooks, A.; Farquhar, G.D. Effect of Temperature on the CO₂/O₂ Specificity of Ribulose-1,5-Bisphosphate Carboxylase Oxygenase and the Rate of Respiration in the Light—Estimates from Gas-Exchange Measurements on Spinach. *Planta* **1985**, *165*, 397–406. [[CrossRef](#)] [[PubMed](#)]
65. Sullivan, P.P.; Patton, E.G.; Shaw, R.H.; Finnigan, J.J.; Weil, J.C. Atmospheric Stability Influences on Coupled Boundary Layer and Canopy Turbulence. *J. Atmos. Sci.* **2016**, *73*, 1621–1647.